Drift of scroll waves in thin layers caused by thickness features: asymptotic theory and numerical simulations

I.V. Biktasheva,[1] H. Dierckx,[2] and V.N. Biktashev[3]

[1]*Department of Computer Science, University of Liverpool, Liverpool L69 3BX, UK*
[2]*Department of Mathematical Physics and Astronomy, Ghent University, 9000 Ghent, Belgium*
[3]*College of Engineering, Mathematics and Physical Sciences, University of Exeter, Exeter EX4 4QF, UK*
(Dated: January 15, 2015)

A scroll wave in a very thin layer of excitable medium is similar to a spiral wave, but its behaviour is affected by the layer geometry. We identify the effect of sharp variations of the layer thickness, which is separate from filament tension and curvature-induced drifts described earlier. We outline a two-step asymptotic theory describing this effect, including asymptotics in the layer thickness and calculation of the drift of so perturbed spiral waves using response functions. As specific examples, we consider drift of scrolls along thickness steps, ridges, ditches, and disk-shaped thickness variations. Asymptotic predictions agree with numerical simulations.

Spiral waves in two dimensions (2D) and scroll waves in three dimensions (3D) are regimes of self-organization observed in physical, chemical and biological spatially-extended dissipative systems with excitable or self-oscillatory properties [1]. A particularly important example are the re-entrant waves of excitation underlying arrhythmias in the heart [2]. In nature, 2D systems often are very thin 3D layers of the medium, so the dynamic fields vary only slightly in the transmural direction. The geometry of a layer affects the dynamics of scroll waves via the well known phenomena of scroll wave filament tension [3] and surface curvature of the layer [4], which cause scroll waves to drift to or from thinner regions and more curved regions respectively. There are, however, effects not reducible to these phenomena, and rather related to *sharp features* of the layer thickness. Fig. 1 shows a paradoxical example of a scroll wave with a *positive* filament tension first attracted towards the *thicker* part of the layer and then drifting along the thickness step. There is experimental evidence that sharp thickness variations can play a significant role in atrial fibrillation [5, 6].

In this Letter, we present an asymptotic theory of drift of scroll waves caused by variations of layer thickness. Predictions of this theory are quantitatively confirmed by direct numerical simulations for two selected archetypical models, one excitable and one self-oscillatory. We demonstrate that sharp variations can produce drifts that are not reducible to filament tension and surface curvature. The details of these drifts depend on the reaction-diffusion kinetics, as well as the size, geometry and position of the thickness feature. A typical motif, observed for both selected models, is that a scroll is first attracted towards a sharp thickness variation and then drifts along or around it.

We start from a generic homogeneous isotropic reaction-diffusion system in 3D:

$$\mathbf{v}_t = \mathbf{f}(\mathbf{v}) + \mathbf{D}\nabla^2\mathbf{v}, \qquad (1)$$

where $\mathbf{v} = [u(\vec{r}, t), v(\vec{r}, t)]^T$, $\vec{r} = (x, y, z)$. In numerical examples, we use excitable FitzHugh-Nagumo system [7], with
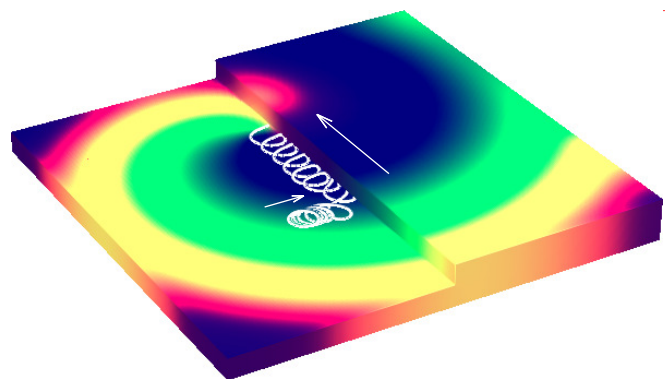

FIG. 1. Surface view of a scroll wave in a thin layer of excitable medium described by FitzHugh-Nagumo system (1,2), with a step-wise variation of thickness. White curve is the trace of the vortex filament appearing at the top surface [9].

kinetics

$$\mathbf{f} : \begin{bmatrix} u \\ v \end{bmatrix} \mapsto \begin{bmatrix} \alpha^{-1}(u - u^3/3 - v) \\ \alpha(u + \beta - \gamma v) \end{bmatrix} \qquad (2)$$

for $\alpha = 0.3$, $\beta = 0.68$, $\gamma = 0.5$, and $\mathbf{D} = \mathrm{diag}(1, 0)$, and self-oscillatory Oregonator model of the Belousov-Zhabotinsky reaction [8], with kinetics

$$\mathbf{f} : \begin{bmatrix} u \\ v \end{bmatrix} \mapsto \begin{bmatrix} p^{-1}\left(u(1-u) - fv\frac{u-q}{u+q}\right) \\ u - v \end{bmatrix} \qquad (3)$$

for $p = 0.1$, $f = 1.5$, $q = 0.002$, and $\mathbf{D} = \mathrm{diag}(1, 0.6)$ [9].

We consider system (1) in a thin layer, $z \in [z_{\min}(x, y), z_{\max}(x, y)]$, $(x, y) \in \mathbb{R}^2$, with no-flux boundaries at $z = z_{\min}$ and $z = z_{\max}$. Let $H(x, y) \equiv z_{\max}(x, y) - z_{\min}(x, y)$ and $0 < H(x, y) \leq \mu \ll 1$. Then $\mathbf{v}(x, y, z, t) = \mathbf{u}(x, y, t) + \mathcal{O}(\mu^2)$ [9], and Eq. (1) in the leading order in μ reduces to the following 2D approximation:

$$\mathbf{u}_t = \mathbf{f}(\mathbf{u}) + \mathbf{D}\frac{1}{H(x, y)}\nabla \cdot (H(x, y)\nabla\mathbf{u}) + \mathcal{O}(\mu^2). \quad (4)$$

We rewrite Eq. (4) in the form

$$\mathbf{u}_t = \mathbf{f}(\mathbf{u}) + \mathbf{D}\nabla^2\mathbf{u} + \epsilon\mathbf{h}(\mathbf{u}, x, y, \nabla) \tag{5}$$

where

$$\epsilon\mathbf{h} = \epsilon\mathbf{D}\left(\nabla K\right)\cdot\left(\nabla\mathbf{u}\right), \qquad \epsilon K = \ln H. \tag{6}$$

Eqs. (5,6) will be treated as a perturbation problem with the formal small parameter ϵ, distinct from the small parmeter μ. So, for Eq. (5) we assume existence of a rigidly rotating spiral wave solution $\mathbf{U}$ at $\epsilon = 0$.

In what follows, we explicitly calculate scroll wave drift for three given geometries corresponding to abrupt changes in domain thickness, i.e. a thickness step, ditch, and circular bulge. First, we consider a step in thickness, as in Fig. 1:

$$H(x,y) = \begin{cases} H_+, & x > x_s, \\ H_-, & x < x_s. \end{cases} \tag{7}$$

Since $K = K(x)$, one has $\epsilon\mathbf{h} = \epsilon\mathbf{D}K_x\mathbf{u}_x$. With Θ the Heaviside step function, we have $\epsilon K = \ln\left(H_-\right) + \epsilon\,\Theta(x - x_s)$, $\epsilon = \ln(H_+/H_-)$, such that

$$\epsilon\mathbf{h} = \epsilon\,\delta(x - x_s)\mathbf{D}\mathbf{u}_x. \tag{8}$$

Eqs. (12,13,14) of [10] predict the drift velocity $\epsilon F(\vec{R}) = \epsilon\left(F_x + iF_y\right)$ as overlap integrals of translational response functions:

$$\frac{d\vec{R}}{dt} = \epsilon\vec{F}(\vec{R}) = \epsilon\left(F_x, F_y\right), \tag{9}$$

$$F(\vec{R}) = \int\limits_0^\infty \oint \mathbf{W}\left(r, \theta\right)^\dagger \boldsymbol{\alpha}(r, \theta; \vec{R})\, d\theta\, r dr, \tag{10}$$

$$\boldsymbol{\alpha}(r, \theta; \vec{R}) = \oint e^{-i\phi}\,\tilde{\mathbf{h}}(\mathbf{U}, r, \theta, \phi)\,\frac{d\phi}{2\pi}, \tag{11}$$

where $\tilde{\mathbf{h}}$ is the perturbation $\mathbf{h}$, calculated for $\mathbf{u} = \mathbf{U}$ and considered in the frame corotating with the spiral, $\mathbf{W}$ are (translational) response functions of the spirals, and $\dagger$ stands for conjugate transposed. Counter-clockwise rotating spirals and their response functions calculated for the two selected models using `DXSpiral` [9, 11] are illustrated in Fig. 5 in [9]; change of chirality of the spirals corresponds to complex conjugation of $\mathbf{W}$, $\boldsymbol{\alpha}$ and F. Evaluation of the integral (11) with account of (8) and the coordinate transformations $\mathbf{h}(\vec{R}, t) = \tilde{\mathbf{h}}(r, \theta, \phi)$, $\vec{R} = (X, Y)$, $\vec{r} = (x, y)$, $d = X - x_s$, $\theta = \vartheta(\vec{r} - \vec{R}) + \phi$, $r = \rho(\vec{r} - \vec{R})$, $x + iy \equiv \rho(\vec{r})\exp(i\vartheta(\vec{r}))$ gives

$$\boldsymbol{\alpha} = \begin{cases} 0, & r \le |d|, \\ \dfrac{\mathbf{D}e^{-i\theta}}{\pi\sqrt{r^2 - d^2}}\left[\dfrac{d^2}{r^2}\,\mathbf{U}_r - \dfrac{i(r^2 - d^2)}{r^3}\,\mathbf{U}_\theta\right], & r > |d|. \end{cases} \tag{12}$$

Eqs. (10) and (12) define the specific force produced by thickness step which depends only on the distance between the current spiral centre and the step and is an even function about the position of the step,

$$F(\vec{R}) = S(d), \qquad d \equiv X - x_s, \tag{13}$$

$$S(-d) = S(d) = S_x(d) + iS_y(d). \tag{14}$$

The components of the function $S(d)$ for the two selected models are shown in Fig. 2(b,e). An important feature are zeros of S_x for $d = \pm d^*$ in both models. Assuming without loss of generality that $x_s = 0$, the drift of a spiral wave is then described asymptotically by

$$\frac{dX}{dt} = \epsilon S_x(X), \quad \frac{dY}{dt} = \epsilon S_y(X), \quad \epsilon = \ln\left(\frac{H_+}{H_-}\right). \tag{15}$$

Fig. 2 illustrates predictions of the theory for the case of a thickness step and their comparison with the direct numerical simulations of both the 2D thickness-reduced system (4) and the full 3D system (1). Numerical simulations for both selected models were done with `BeatBox` [9, 12]. The relevant attractor for (15) is

$$X = -d^*, \qquad Y = Y_0 + \epsilon S_y(-d^*)t, \tag{16}$$

where $S_x(-d^*) = 0$, $S_x{}'(-d^*) < 0$. That is, in both models the spirals attach to the step at its thinner side and drift along with the speed $|\epsilon S_y(-d^*)|$. The speed of the drift is proportional to $\epsilon = \ln(H_+/H_-)$, and the direction of the drift depends on the spiral chirality: compare Fig. 2 (a) and (d).

As a second geometry, let us consider the following thickness profile: for some $x_\ell < x_r$,

$$H(x,y) = \begin{cases} H_o, & x < x_\ell, \\ H_i, & x_\ell < x < x_r, \\ H_o, & x_r < x, \end{cases} \tag{17}$$

which means a "ridge" for $H_i > H_o$ and a "ditch" for $H_i < H_o$. This case is easily reduced to the previous because $H(x,y) = H_i + (H_o - H_i)\left(\Theta(x - x_\ell) - \Theta(x - x_r)\right)$, hence the formal perturbation is $\epsilon\mathbf{h} = \epsilon\left[\delta(x - x_\ell) - \delta(x - x_r)\right]\mathbf{D}\mathbf{u}_x$, where $\epsilon = \ln(H_i/H_o)$. Let $x_\ell = x_s - w/2$, $x_r = x_s + w/2$. We use the linearity of (9)–(11) and the previous result to get the interaction force in the form

$$F(\vec{R}) = T(d; w) = -T(-d; w), \qquad d \equiv X - x_s, \tag{18}$$

$$T = T_x + iT_y = S\left(d + \frac{w}{2}\right) - S\left(d - \frac{w}{2}\right). \tag{19}$$

Fig. 3(a,b) shows the components of $T(d; w)$ for two selected values of the ridge width w, illustrating a pitchfork bifurcation of T_x roots. The bifurcation condition $T_x(d; w) = \partial_d T_x(d; w) = 0$, observation that the bifurcation happens at $d^* = 0$ and evenness of $S(d)$ gives the critical value of the width implicitly as the condition $S_x{}'(w^*/2) = 0$. For the FHN system, there are two positive roots for $S_x{}'(\cdot)$ (see Fig. 2(b)), the smaller giving $w^* \approx 1.769$. For a ditch
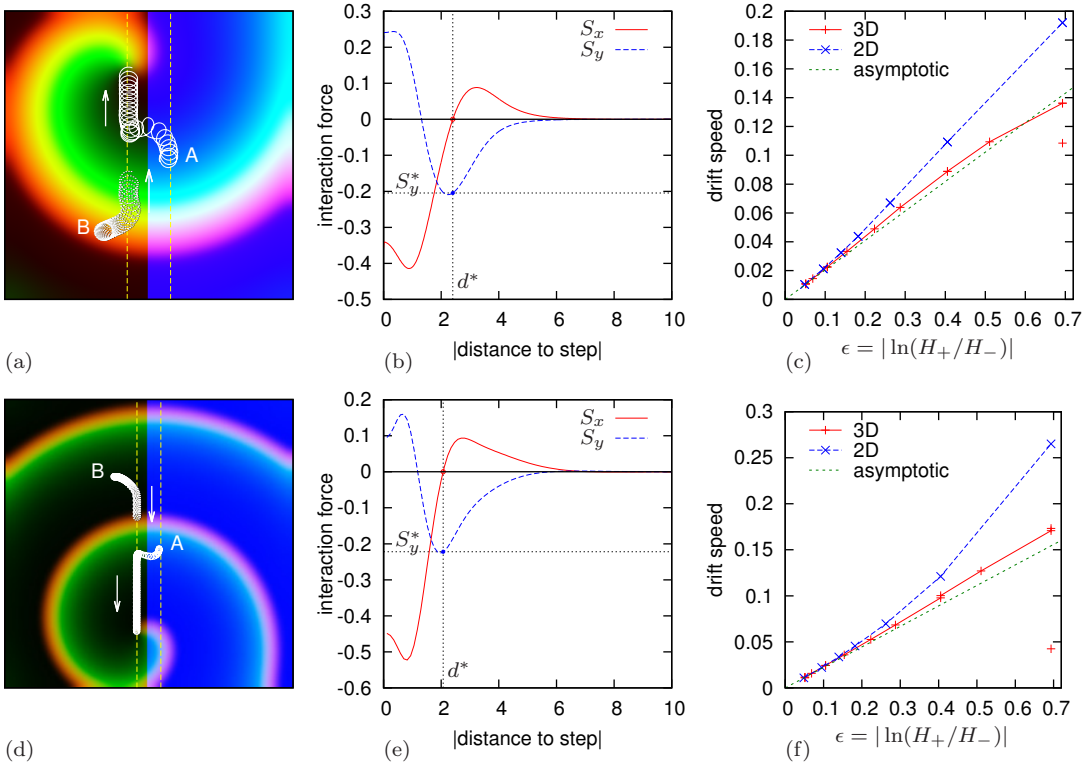
FIG. 2. Asymptotic theory vs numerical simulations for interaction of a scroll wave with a thickness step, for the FitzHugh-Nagumo system (panels a-c) and the Oregonator model (panels d-f). (a,d): Spiral wave snapshot (red color component: u field, green color component: v field, blue color component: H field), with the previous tip path (solid white line) starting at A, another path starting at a different point (B), and loci $d = \pm d^*$ (dashed yellow lines), in 2D system (4). (b,e): Components of the specific force S (14) calculated for counter-clockwise spirals. (c,f): Drift speed along the step in 3D system (1), 2D system (4) and asymptotic predicted by (16).
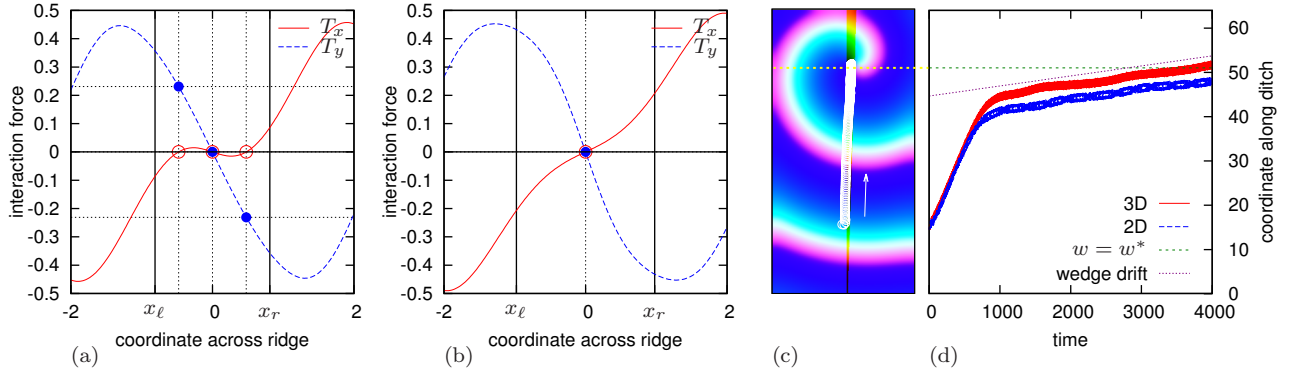

FIG. 3. Results of asymptotic theory of interaction with a ridge/ditch, and comparison with simulations, for FitzHugh-Nagumo system (2). (a,b) Specific interaction force $T(d)$ (19) calculated for counter-clockwise spirals: (a) for $w = 1.621 < w^*$; (b) for $w = 1.953 > w^*$. (c) Spiral wave snapshot (red color component: u field, green color component: v field, blue color component: H field), with the previous tip path (white line) drifting along a cuneiform ditch, of width 0.24 at the lower end, linearly growing to 2.16 at the upper end, box size 32×64, and $H_o/H_i = 1.2$. (d) Coordinate of the spiral tip along the ditch as a function of time. The horizontal dashed line shows location of the ditch width $w = w^*$ corresponding to the point of the pitchfork bifurcation of $T(d; w)$. The slope of the dotted line represents the slow drift speed due to the sides of the ditch being non-parallel.

($\epsilon < 0$), this predicts neutrally stable equilibria along the middle line of the ditch if $w > w^*$ (Fig. 3(b)), and a drift along either side of the ditch, in one direction or the other, depending on the initial condition, if $w < w^*$ (Fig. 3(a)).

Fig. 3(c,d) illustrates the drift along a cuneiform ditch, i.e. a ditch with almost constant but slowly varying width. The coordinate scale along the ditch is the same in both panels, with the bifurcation width w^* designated by the dashed horizontal line. We see that below this line the spiral wave drifts in accordance with the theory and slows down markedly in the

vicinity of this line. It does not stop completely but proceeds further, albeit at a much slower speed, which may be seen as a transient pinning. This slow drift is due to the "wedging" effect of the varying width: at $w \geq w^*$, the forces from the two opposite steps, constituting the banks of the ditch, do not compensate each other exactly due to the angle between them. To estimate roughly the associated correction, let the wedge angle be $\psi \ll 1$. Then the wedge-forced component of the drift speed at the bifurcation point is $2\epsilon S_x(w^*)\sin(\psi/2) \approx \epsilon S_x(w^*)\psi$. For the simulation shown
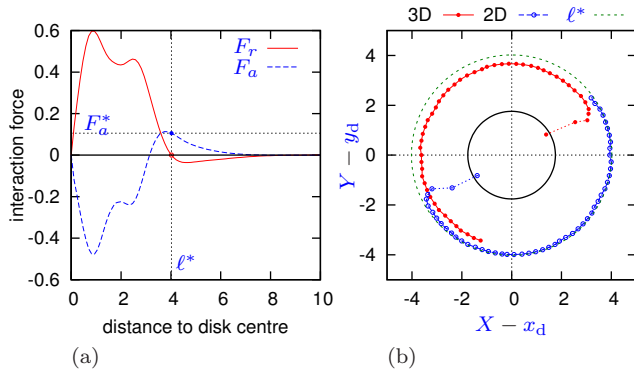
FIG. 4. Interaction of a spiral with a disk-shape bulge in Oregonator model. (a) Components of the interaction force calculated according to (10),(11),(20),(21), for $R_\mathrm{d} = 225/1280 \approx 1.756$. (b) Tip trajectories in simulations of duration corresponding to half of predicted orbiting period (lines as indicated by the legend), together with initial transients (thin dotted lines). The green dashed circle: the theoretically predicted stationary orbit of the spiral centre drift. The black solid circle: the boundary of the bulge.

in Fig. 3(c,d), we have $\psi \approx 0.03$, and $S_x(w^*) \approx 0.4142$, hence the drift speed $\epsilon\psi S_x(w^*) \approx 0.002266$. This wedge-forced drift speed is represented by the dotted line in Fig. 3(d) and agrees well with the simulations. If the initial position of the spiral is where $w \gtrsim w^*$, then it undergoes only the slow, wedge-forced drift from the start (not shown).

Drift caused by ridge or ditch features may help to understand dynamics of scroll waves in atrial geometry, say around pectinate muscles [6]. Another feature, specifically analyzed in [6] by numerical simulations was a circular bulge. To see what our theory can say about that, let us consider thirdly a thickness perturbation of the form

$$H(x,y) = H_0 \left(1 + \epsilon\,\Theta\left(R_\mathrm{d}{}^2 - (x - x_\mathrm{d})^2 - (y - y_\mathrm{d})^2\right)\right)$$

i.e. thickening (for $\epsilon > 0$) or thinning (for $\epsilon < 0$) in a disk-shaped area of radius R_d. Then we have

$$\boldsymbol{\alpha} = \frac{\mathrm{e}^{\mathrm{i}\vartheta_0}\mathrm{e}^{-\mathrm{i}\theta}\mathbf{D}}{\pi r\ell\sqrt{1-\kappa^2}}\left[(\ell\kappa^2 + r\kappa)\,\mathbf{U}_r - \frac{\mathrm{i}\ell(1-\kappa^2)}{r}\,\mathbf{U}_\theta\right] \quad (20)$$

for $\vec{r} \in (|R_\mathrm{d} - \ell|, R_\mathrm{d} + \ell)$, and $\boldsymbol{\alpha} = 0$ otherwise. Here $\ell\mathrm{e}^{\mathrm{i}\vartheta_0} = (x_\mathrm{d} - X) + \mathrm{i}(y_\mathrm{d} - Y)$ represents the vector from the current spiral centre (X, Y) to the bulge centre $(x_\mathrm{d}, y_\mathrm{d})$, and $\kappa = \left(R_\mathrm{d}{}^2 - \ell^2 - r^2\right)/(2r\ell)$. Hence the interaction force is

$$F_x + \mathrm{i}F_y = \mathrm{e}^{\mathrm{i}\vartheta_0}\left(F_r(\ell) + \mathrm{i}F_a(\ell)\right). \quad (21)$$

The radial $F_r(\ell)$ and the azimuthal $F_a(\ell)$ components calculated for the Oregonator model (3) for an arbitrarily chosen disk radius R_d are shown in Fig. 4(a). We observe there is a root of $F_r(\ell)$ at $\ell = \ell^* \approx 4.023$ and the corresponding value of the specific force $F_a^* = F_a(\ell^*) \approx 0.1055$ predicts long-term behaviour of a spiral starting from an appropriate initial condition as "meander" or "orbital movement" along a circle of radius ℓ^* with the linear speed ϵF_a^*, and an orbit

period of $2\pi\ell^*/(\epsilon F_a^*) \approx 1314$. Fig. 4(b) compares these predictions with results of 2D and 3D numerical simulations at $\epsilon = \log(1.2)$. This result is similar to the case considered phenomenologically in [6] and is analogous to "orbital motion" described in [13] for localized parametric heterogeneities.

To summarise, the movement of transmural scroll waves through thin layers of excitable media of varying thickness can be approximately described by thickness-averaged two-dimensional equations, and a corresponding 2D perturbation theory can be successfully applied within its limits. Our theory shows the propensity of scrolls to interact with sharp features of the layer geometry. In the examples considered, this interaction caused a scroll to position itself at a certain distance from a sharp feature and drift along/around it with the speed determined by the feature's magnitude, measured by the relative variation of the thickness. This is distinct from and not reducible to previously known geometric effects such as filament tension or curvature-induced drift, and is completely independent from other factors that may cause drift, such as parametric inhomogeneities or external forcing (see e.g. [10]). Interaction with sharp features can manifest nontrivial attractor structures, depending on the geometric parameters. These predictions should be immediately testable in experiments with the Belousov-Zhabotinsky reaction, can be used in experiments, say for precision positioning of scrolls, and may have important implications for understanding the evolution of re-entrant waves of excitation in the heart, particularly in atria which have an abundance of geometric features. For instance, our results give a theoretical explanation, and hence suggest a universal character of scroll wave "anchoring" and "meandering" caused by thickness variations, which are implicated in perpetuation of atrial fibrillation [6].

[1] A. M. Zhabotinsky and A. N. Zaikin, in *Oscillatory processes in biological and chemical systems*, edited by E. E. Selkov, A. A. Zhabotinsky, and S. E. Shnol (Nauka, Pushchino, 1971) p. 279; M. A. Allessie, F. I. M. Bonke, and F. J. G. Schopman, Circ. Res. **33**, 54 (1973); F. Alcantara and M. Monk, J. Gen. Microbiol. **85**, 321 (1974); N. A. Gorelova and J. Bures, J. Neurobiol. **14**, 353 (1983); B. F. Madore and W. L. Freedman, Am. Sci. **75**, 252 (1987); S. Jakubith, H. H. Rotermund, W. Engel, A. von Oertzen, and G. Ertl, Phys. Rev. Lett. **65**, 3013 (1990); J. Lechleiter, S. Girard, E. Peralta, and D. Clapham, Science **252** (1991); T. Frisch, S. Rica, P. Coullet, and J. M. Gilli, Phys. Rev. Lett. **72**, 1471 (1994); M. C. Cross and P. C. Hohenberg, Rev. Mod. Phys. **65**, 851 (1993).
[2] F. H. Fenton, E. M. Cherry, and L. Glass, Scholarpedia **3**, 1665 (2008).
[3] V. N. Biktashev, A. V. Holden, and H. Zhang, Phil. Trans. Roy. Soc. Lond. ser. A **347**, 611 (1994).
[4] H. Dierckx, E. Brisard, H. Verschelde, and A. V. Panfilov, Phys.

Rev. E **88**, 012908 (2013).

[5] T. J. Wu, M. Yashima, F. Xie, C. A. Athill, Y. H. Kim, M. C. Fishbein, Z. Qu, A. Garfinkel, J. N. Weiss, H. S. Karagueuzian, and P. S. Chen, Circulation Research **83**, 448 (1998).

[6] M. Yamazaki, S. Mironov, C. Taravant, J. Brec, L. M. Vaquero, K. Bandaru, U. M. R. Avula, H. Honjo, I. Kodama, O. Berenfeld, and J. Kalifa, Cardiovascular Research **94**, 48 (2012).

[7] R. FitzHugh, Biophys. J. **1**, 445 (1961); J. Nagumo, S. Arimoto, and S. Yoshizawa, Proc. IRE **50**, 2061 (1962); A. T. Winfree, Chaos **1**, 303 (1991).

[8] R. J. Field and R. M. Noyes, J. Chem. Phys. **60**, 1877 (1974); J. J. Tyson and P. C. Fife, *ibid*. **73**, 2224 (1980).

[9] See EPAPS Document No. [number will be inserted by publisher] for details of asymptotic and numerical procedures. For more information on EPAPS, see `http://www.aip.org/pubservs/epaps.html`.

[10] I. V. Biktasheva, D. Barkley, V. N. Biktashev, and A. J. Foulkes, Phys. Rev. E **81**, 066202 (2010).

[11] I. V. Biktasheva, D. Barkley, V. N. Biktashev, G. V. Bordyugov, and A. J. Foulkes, Phys. Rev. E **79**, 056702 (2009), `http://www.csc.liv.ac.uk/~ivb/software/DXSpiral.html`.

[12] R. McFarlane and I. V. Biktasheva, in *BCS International Academic Conference "Visions of Computer Science"* (Imperial College London, 2008) `http://empslocal.ex.ac.uk/people/staff/vnb262/software/BeatBox/`.

[13] V. N. Biktashev, D. Barkley, and I. V. Biktasheva, Phys. Rev. Lett. **104**, 058302 (2010).

Supplementary material:
Drift of scroll waves in thin layers caused by thickness features
I.V. Biktasheva, H. Dierckx, V.N. Biktashev

Thin layer asymptotics

When the thickness of the excitable medium layer is much smaller than the diffusion length $\sqrt{||\mathbf{D}||/\max(||\partial\mathbf{f}/\partial\mathbf{v}||)}$, then we can expect the concentration field $\mathbf{v}$ to be nearly constant across the thickness of the layer, thus being effectively a two-dimensional field. This is, of course, "intuitively obvious", and simple considerations based on conservation of matter can help to immediately "guess" the resulting equation (4). We, however, would like to also have some estimate of the accuracy of that reduced equation, in order to know its limitations, so we feel that a simple guess is not quite sufficient. Problems for partial differential equations posed in thin or slender domains occur in many fields of applied mathematics and there are many works considering such problems in various situations and with various practical purposes. In this respect we mention two examples: E. Yanagida, "Existence of stable stationary solutions of scalar reaction-diffusion equations in thin tubular domains", *Applicable Analysis* **36**:171-188 (1990), and J. K. Hale and G. Raugel, "Reaction-diffusion equations on thin domains", *J. Math. pures et appl.* **71**:33–95 (1992), in which the reduction has been done rigorously and in the context of reaction-diffusion equations, making them particularly close to what we require for our study. However those rigorous results have been obtained under certain assumptions which make them technically inapplicable to our case. So, Yanagida (1990) writes about "tubular" domains, that is, there is only one "long" dimension. It is also focused on studying stationary solutions, and presented for the case of one-component reaction-diffusion system. All of these assumptions are essential for their results, and all of them are unsuitable for us, as the spiral wave solutions require two spatial dimensions, at least two components and are non-stationary. The work by Hale and Raugel (1992) goes further in that it allows up to two long dimensions and considers non-stationary solutions, but it is still restricted to one-component reaction-diffusion systems with extra requirements on the kinetic term. We are not aware of either rigorous or formal results that would quite cover our needs, hence we present our own derivation, even though it is only a formal asymptotic.

To exclude the effects of the curvature we assume the layer to be flat on the macroscopic scale. The formal setup is as follows:

$$\partial_t \mathbf{v} = \mathbf{D}\nabla^2 \mathbf{v} + \mathbf{f}(\mathbf{v}), \qquad (x,y) \in \mathbb{R}^2, \qquad z \in (z_{\min}(x,y;\mu), z_{\max}(x,y;\mu),$$
$$z_{\min}(x,y;\mu) = 0, \qquad z_{\max}(x,y;\mu) = H(x,y;\mu) = \mu\tilde{H}(x,y), \qquad \mu \ll 1,$$
$$\vec{n}(z_{\min}) \cdot \mathbf{D}\nabla\mathbf{v}(x,y,z_{\min}) = 0,$$
$$\vec{n}(z_{\max}) \cdot \mathbf{D}\nabla\mathbf{v}(x,y,z_{\max}) = 0,$$

where $\vec{n}(\cdot)$ is the normal vector at the corresponding surface. The shape of the layer is asymmetric and it may seem that variations of thickness may introduce small curvature effects; however it is easy to see that the above formulation is exactly equivalent to a symmetric one,

$$z_{\min}(x,y;\mu) = -\mu\tilde{H}(x,y), \qquad z_{\max}(x,y;\mu) = \mu\tilde{H}(x,y).$$

The boundary conditions at $z = z_{\min}$, $z = z_{\max}$ mean that the flux lines for the $\mathbf{v}$ concentrations need to intersect the domain boundary perpendicularly. To accommodate this property in our asymptotic solution, we switch from the original Cartesian coordinates $\vec{r} = (x^j) = (x,y,z)$ to new curvilinear coordinates $(\rho^j) = (\xi,\eta,\zeta)$, $j = 1,2,3$, in the following way:

- Coordinate ζ is "transmural", that is

$$z(\xi,\eta,0) = z_{\min}(x(\xi,\eta,0), y(\xi,\eta,0)), \qquad z(\xi,\eta,1) = z_{\max}(x(\xi,\eta,1), y(\xi,\eta,1)). \tag{22}$$

- The other two "intramural" coordinates (ξ,η) are chosen locally orthogonal to ζ, i.e.

$$\frac{\partial\vec{r}}{\partial\xi} \cdot \frac{\partial\vec{r}}{\partial\zeta} = \frac{\partial\vec{r}}{\partial\eta} \cdot \frac{\partial\vec{r}}{\partial\zeta} = 0. \tag{23}$$

- The intramural coordinates match the horizontal Cartesian coordinates in the sense that

$$x(\xi,\eta,0) = \xi, \qquad y(\xi,\eta,0) = \eta. \tag{24}$$

Thus the choice of the curvilinear coordinates is fully determined by the choice of function $\zeta(\vec{r})$. A convenient choice is "heat coordinates", when $\zeta(\vec{r}) = T(\vec{r}; \mu)$ which is a solution of the boundary-value problem

$$\nabla^2 T(x, y, z) = 0, \qquad z \in (0, \mu\tilde{H}(x, y));$$
$$T(x, y, 0) = 0,$$
$$T(x, y, \mu\tilde{H}(x, y)) = 1, \tag{25}$$

i.e. it is identified with an established temperature distribution when a unit temperature drop is imposed across the layer. Then the lines $\xi = \text{const}, \eta = \text{const}$ can be interpreted as the lines of heat flux, and in the new coordinates, the boundary conditions become simply condition of zero derivative in ζ, as the vectors $\vec{n}$ are tangent to these flux lines. The two leading terms of the asymptotic of the solution of (25) are

$$T = \frac{z}{\mu\tilde{H}} + \frac{\mu^2 \tilde{H}^2}{6} \left(1 - \frac{z^2}{\mu^2 \tilde{H}^2}\right) \frac{z}{\mu\tilde{H}} \left((\nabla L)^2 - \nabla^2 L\right) + \mathcal{O}\left(\mu^4\right); \qquad \left(z \in [0, \mu\tilde{H}]\right)$$

where

$$\tilde{H} = \tilde{H}(x, y), \qquad L = L(x, y) = \ln \tilde{H}(x, y).$$

Let g_{jk} be the metric tensor in the curvilinear coordinates ρ^j, that is

$$g_{jk} = \frac{\partial \vec{r}}{\partial \rho^j} \cdot \frac{\partial \vec{r}}{\partial \rho^k} = g_{kj}.$$

Due to the local orthogonality condition (23), we have automatically $g_{13} = g_{23} = 0$, and the metric tensor takes the block-diagonal form

$$\left[\, g_{jk} \,\right] = \begin{bmatrix} h_{11} & h_{12} & 0 \\ h_{21} & h_{22} & 0 \\ 0 & 0 & g_{33} \end{bmatrix}$$

To find the asymptotics of the remaining components of the metric tensor, we first find $\vec{r}(\zeta)$ as a solution of a Cauchy problem for the ODE system, defined by function $T(\vec{r})$ found previously and depending on $\rho^{1,2}$ as parameters,

$$\frac{\partial \vec{r}}{\partial \zeta} = \lambda(\zeta)\nabla T(\vec{r}) \tag{26}$$

$$T(\vec{r}(\rho^j)) \equiv \zeta, \tag{27}$$

$$\vec{r}(0) = (\xi, \eta, 0). \tag{28}$$

The asymptotics for the solution are

$$\lambda = \mu^2 \tilde{H}^2(\xi, \eta) + \mathcal{O}\left(\mu^4\right),$$
$$x = \xi - \frac{1}{2}\mu^2 \tilde{H}\tilde{H}_x \zeta^2 + \mathcal{O}\left(\mu^4\right),$$
$$y = \eta - \frac{1}{2}\mu^2 \tilde{H}\tilde{H}_y \zeta^2 + \mathcal{O}\left(\mu^4\right),$$
$$z = \mu\tilde{H}\,\zeta - \frac{1}{6}\mu^3 \tilde{H}^3 \left[(\nabla L)^2 \left(\zeta + 2\zeta^3\right) - \nabla^2 L \left(\zeta - \zeta^3\right)\right] + \mathcal{O}\left(\mu^5\right),$$

where $\tilde{H}$, L and their derivatives are evaluated at (ξ, η). This then leads to the asymptotics of the components of the metric tensor in the form

$$h_{ab} = \delta_{ab} + \mathcal{O}\left(\mu^2\right), \qquad a, b = 1, 2,$$
$$g_{33} = \mu^2 \tilde{H}^2 - \frac{1}{3}\mu^4 \tilde{H}^4 \left[(\nabla L)^2 \left(1 + 3\zeta^2\right) - \nabla^2 L \left(1 - 3\zeta^2\right)\right] + \mathcal{O}\left(\mu^6\right).$$

Here for g_{33} we go beyond the leading term; the reason for that will become clearer later.

For the curvilinear Laplacian we shall also need

$$|g| = \det\left[\,g_{jk}\,\right] = g_{33}\det\left[\,h_{ab}\,\right] = \mu^2\tilde{H}^2 + \mathcal{O}\left(\mu^4\right),$$

and

$$\left[\,g^{jk}\,\right] = \left[\,g_{jk}\,\right]^{-1} = \left[\begin{array}{cc} \left[\,h_{ab}\,\right] & \mathbf{0} \\ \mathbf{0}^{\mathrm{T}} & g_{33} \end{array}\right]^{-1} = \left[\begin{array}{cc} \left[\,h_{ab}\,\right]^{-1} & \mathbf{0} \\ \mathbf{0}^{\mathrm{T}} & g_{33}^{-1} \end{array}\right] = \left[\begin{array}{cc} \left[\,h^{ab}\,\right] & \mathbf{0} \\ \mathbf{0}^{\mathrm{T}} & g^{33} \end{array}\right],$$

where

$$h^{ab} = \delta^{ab} + \mathcal{O}\left(\mu^2\right),$$

and

$$g^{33} = \frac{1}{\mu^2\tilde{H}^2} + \frac{1}{3}\left[(\nabla L)^2\left(1 + 3\zeta^2\right) - \nabla^2 L\left(1 - 3\zeta^2\right)\right] + \mathcal{O}\left(\mu^2\right).$$

Here we see the reason for a higher accuracy: the second term of the asymptotic for g^{33} has order $\mathcal{O}\left(1\right)$ so omitting it could have affected our main result.

Now we are ready to calculate the Laplacian of the concentration field, which in the new curvilinear coordinates is represented by the Laplace-Beltrami operator (using Einstein summation convention)

$$\nabla^2\mathbf{v} = |g|^{-1/2}\frac{\partial}{\partial\rho^j}\left(|g|^{1/2}g^{jk}\frac{\partial\mathbf{v}}{\partial\rho^k}\right).$$

Taking into account the results obtained above, this works out to be

$$\nabla^2\mathbf{v} = \frac{1}{\mu^2\tilde{H}^2}\mathbf{v}'' + \nabla L\nabla\mathbf{v} + \nabla^2\mathbf{v} + G\,\mathbf{v}'' + \mathcal{O}\left(\mu^2\right)$$

where

$$G = G(\xi,\eta,\zeta) = \left(\frac{1}{3} + \zeta^2\right)(\nabla L)^2 - \left(\frac{1}{3} - \zeta^2\right)\nabla^2 L.$$

On the right-hand side, functions $\tilde{H}$, L and their derivatives are evaluated at (ξ,η), ∇ is the gradient operator in the (ξ,η) plane and the prime $'$ stands for differentiation by ζ.

The reaction-diffusion equation in the new coordinates then takes the form

$$\partial_t\mathbf{v} = \mathbf{D}\left[\frac{1}{\mu^2\tilde{H}^2}\mathbf{v}'' + \nabla L\nabla\mathbf{v} + \nabla^2\mathbf{v} + G\,\mathbf{v}'' + \mathcal{O}\left(\mu^2\right)\right] + \mathbf{f}(\mathbf{v})$$

with the boundary conditions

$$\mathbf{D}\partial_3\mathbf{v}(\xi,\eta,0,t) = \mathbf{D}\partial_3\mathbf{v}(\xi,\eta,1,t) = 0.$$

We shall look for the solution of this problem in the form of an asymptotic series in μ^2, and consider the two leading terms,

$$\mathbf{v}(\xi,\eta,\zeta,t;\mu) = \mathbf{u}(\xi,\eta,\zeta,t) + \mu^2\mathbf{g}(\xi,\eta,\zeta,t) + \mathcal{O}\left(\mu^4\right).$$

Upon rewriting our problem in the form

$$\mathbf{D}\left(\mathbf{u} + \mu^2\mathbf{g}\right)'' = \mu^2\tilde{H}^2\left[\partial_t\left(\mathbf{u} + \mu^2\mathbf{g}\right) - \frac{1}{\tilde{H}}\mathbf{D}\nabla\left(\tilde{H}\nabla\left(\mathbf{u} + \mu^2\mathbf{g}\right)\right) - G\mathbf{D}\left(\mathbf{u}'' + \mu^2\mathbf{g}''\right) - \mathbf{f}\left(\mathbf{u} + \mu^2\mathbf{g}\right)\right] + \mathcal{O}\left(\mu^4\right),$$

$$\left[\mathbf{D}(\mathbf{u} + \mu^2\mathbf{g})'\right]_{\zeta=0,1} = \mathcal{O}\left(\mu^4\right),$$

we get in the order $\mathcal{O}\left(1\right)$

$$\mathbf{D}\mathbf{u}'' = 0,\qquad \left[\mathbf{D}\mathbf{u}'\right]_{\zeta=0,1} = 0,$$

wherefrom $\mathbf{u}' = \partial_\zeta \mathbf{u} \equiv 0$, i.e. function $\mathbf{u}$ depends only on ξ, η and t but not on ζ, as expected. Further, in the order $\mathcal{O}\left(\mu^2\right)$ we have

$$\mathbf{D}\mathbf{g}'' = \tilde{H}^2 \left[\partial_t \mathbf{u} - \frac{1}{\tilde{H}}\mathbf{D}\nabla\left(\tilde{H}\nabla\mathbf{u}\right) - \mathbf{D}G\mathbf{u}'' - \mathbf{f}(\mathbf{u})\right], \qquad [\mathbf{D}\mathbf{g}']_{\zeta=0,1} = 0.$$

This is a two-point ODE boundary-value problem for $\mathbf{g}(\zeta)$ depending on ξ, η and t as parameters. Note that the term $\mathbf{D}G\mathbf{u}''$ vanishes by the $\mathcal{O}\left(1\right)$ result, and the remaining free term is a constant, i.e. does not depend on ζ. This problem is solvable if this constant vanishes, i.e.

$$\partial_t \mathbf{u} - \frac{1}{\tilde{H}}\mathbf{D}\nabla\left(\tilde{H}\nabla\mathbf{u}\right) - \mathbf{f}(\mathbf{u}) = 0$$

which gives the leading term for the equation (4) of the main text, since $\nabla\tilde{H}/\tilde{H} = \nabla H/H$.

The higher-order approximations cannot be obtained within the same asymptotic procedure, and instead one would need to look for the asymptotic expansion of the right-hand side of the evolution equation for $\mathbf{u}$, that is, $\partial_t \mathbf{u} = \sum_n \mu^{2n}\hat{\mathbf{u}}_n(\mathbf{u}, H, \nabla)$, i.e. admit different asymptotic orders in the right-hand side of the "master equation". Such asymptotic technique is outlined e.g. in V.N. Biktashev, "Envelope Equations for Modulated Non-conservative Waves", in *IUTAM Symposium Asymptotics, Singularities and Homogenisation in Problems of Mechanics*, pp. 525-535, ed. by A.B. Movchan, Kluwer, Dordrecht-Boston-London, 2003, `http://empslocal.ex.ac.uk/people/staff/vnb262/publ/iutam-2002/index.html`. We do not present the resulting derivation here as it is tedious and its precise results are not required in the main part of the paper; however the most important fact is that the next-to-leading order terms in the evolution equation are $\mathcal{O}\left(\mu^2\right)$, and this fact is already evident from the above.

The above derivation was done under the assumption of smoothness of the thickness profile $\tilde{H}(x, y)$. Hence the applications considered in the main paper will be formally covered by this approximation and the 2D spiral perturbation theory, if the "sharp features" considered there are smooth on the scale of $\tilde{H}$ but sharper than the typical scale of the effective response functions' support. Deviation from this condition in actual 3D simulations may account for some of the discrepancies between the 3D and 2D simulations.

Response functions quadratures

Straight step

The function (12) has a singularity at $r = |d|$, so the resulting integral by r cannot be adequately evaluated by the usual trapezoidal rule. So we proceed instead in the following way. Let the radii grid be $r \in \{j\Delta\rho \mid j = 0, 1, 2\dots\}$, and $|d| = k\Delta\rho$ for some $k \in \mathbb{Z}_+$. Then, for a regular function $f(r)$ and a constant $\sigma > -1$, we can write

$$\int_{|d|}^\infty f(r)(r^2 - d^2)^\sigma \, \mathrm{d}r = \int_{|d|}^\infty F(r)(r - d)^\sigma \, \mathrm{d}r = \sum_{j=k}^\infty \int_{j\Delta\rho}^{(j+1)\Delta\rho} F(r)(r - d)^\sigma \, \mathrm{d}r \approx \sum_{j=k}^\infty C_j f_j \Delta\rho,$$

where $F(r) = f(r)(r + d)^\sigma$, $f_j = f(j\Delta\rho)$, and linear interpolation of $F(r)$ within each subinterval gives

$$C_j = \begin{cases} \frac{\Delta\rho^{2\sigma}}{2(\sigma+1)}(2k)^\sigma, & j = k, \\ \frac{\Delta\rho^{2\sigma}}{2(\sigma+1)}\left[(j - k + 1)^{\sigma+1} - (j - k - 1)^{\sigma+1}\right](j + k)^\sigma, & j > k. \end{cases}$$

For $\sigma = -1/2$,

$$C_j = \begin{cases} 0, & j < k, \\ \frac{1}{\Delta\rho\sqrt{2k}}, & j = k, \\ \frac{1}{\Delta\rho\sqrt{j+k}}\left[\sqrt{j - k + 1} - \sqrt{j - k - 1}\right], & j > k. \end{cases} \tag{29}$$

In other words, we can use the usual trapezoidal formula, but should multiply $f_j = f(j\Delta\rho)$ by coefficients C_j given above instead of $(r^2 - d^2)^{-1/2} = (r^2 - d^2)^\sigma = (j^2 - k^2)^\sigma\Delta\rho^{2\sigma} = (j^2 - k^2)^{-1/2}\Delta\rho^{-1}$.

Circular step

Similarly, the quadrature for interaction with a disk involves α described by (20), and so is also singular, as it contains denominator $\sqrt{1 - \kappa^2}$ which becomes zero at both ends of the integration interval:

$$\sqrt{1 - \kappa^2} = \frac{1}{2r\ell} \left[(r - r_{\min})(r_{\max} - r)(r + r_{\min})(r + r_{\max}) \right]^{1/2}$$

where $r_{\min} = |R_{\mathrm{d}} - \ell|$, $r_{\max} = |R_{\mathrm{d}} + \ell|$. Doing as before, we get

$$\int_{r_{\min}}^{r_{\max}} \frac{F(r)}{\sqrt{(r - r_{\min})(r_{\max} - r)}}\, \mathrm{d}r = \sum_{j=0}^{N} C_j F(r_j)\, \Delta\rho,$$

where

$$C_0 = \frac{1}{\Delta\rho^2} \left[(A_0 - A_1)(r_1 - r_{\mathrm{mid}}) + R_0 - R_1 \right],$$

$$C_j = \frac{1}{\Delta\rho^2} \left[(A_j - A_{j+1})(r_{j+1} - r_{\mathrm{mid}}) + (A_j - A_{j-1})(r_{j-1} - r_{\mathrm{mid}}) + 2R_j - R_{j+1} - R_{j-1} \right],\ j = 1, \ldots, N-1,$$

$$C_N = \frac{1}{\Delta\rho^2} \left[(A_N - A_{N-1})(r_{N-1} - r_{\mathrm{mid}}) - R_{N-1} + R_N \right],$$

$$r_{\mathrm{mid}} = \frac{1}{2}(r_{\min} + r_{\max}),$$

$$\Delta\rho = (r_{\max} - r_{\min})/N,$$

$$\vec{r}_j = r_{\min} + j\Delta\rho, \qquad j = 0, \ldots, N,$$

$$R_j = \sqrt{(r_{\max} - r_j)(r_j - r_{\min})},$$

$$A_j = \arcsin\left(\frac{2(r_j - r_{\mathrm{mid}})}{r_{\max} - r_{\min}} \right).$$

Discretization

Two-dimensional simulations

We use explicit Euler timestepping with time step Δt and central differencing for the diffusion term in (4), with the following discretization scheme

$$\left[\frac{1}{\tilde{H}} \nabla \cdot \left(\tilde{H} \nabla \mathbf{u} \right) \right]_{i,j} = \frac{1}{2\Delta x^2} \frac{1}{\tilde{H}_{i,j}} \sum_{(i',j') \in I} \left(\tilde{H}_{i+i',j+j'} + \tilde{H}_{i,j} \right) \left(\mathbf{u}_{i+i',j+j'} - \mathbf{u}_{i,j} \right)$$

where (i, j) are 2D indices of the regular space grid of the size $N_x \times N_y$ with step Δx and $I = \{(-1, 0), (1, 0), (0, -1), (0, 1)\}$. We employ standard non-flux boundary conditions. The discretization parameters used for different results are described in Table I.

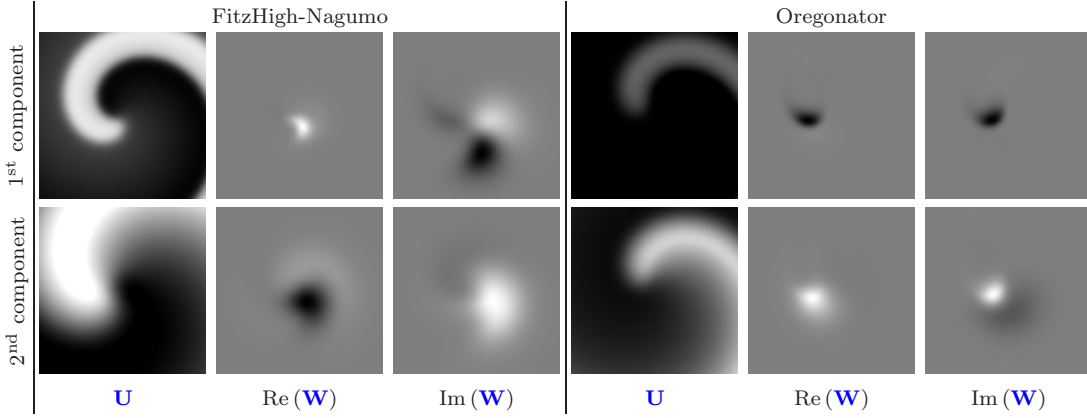| Figure	Δt	Δx	N_x	N_y
2(a,c)	6.4×10^{-4}	8×10^{-2}	400	400
2(d,f)	0.25	1.5×10^{-3}	200	200
3(c,d)	6.4×10^{-4}	8×10^{-2}	400	800
4(b)	0.25	1.5×10^{-3}	200	200

TABLE I. Discretization parameters in 2D simulations

FIG. 5. Density plots of the spiral waves $\mathbf{U}$ and response functions $\mathbf{W}$ of the FitzHugh-Nagumo system (2) (central fragment 12.5×12.5) and Oregonator model (3) (central fragment 15×15). Grey periphery of $\mathbf{W}$ components corresponds to zero, i.e. $\mathbf{W}$ are well localized ensuring convergence of integrals (10).

Three-dimensional simulations

The discretization in 3D is a natural extension of the 2D scheme, except instead of a fancy diffusion operator of (4) we now have the plain diffusion of (1). The complication now comes from the more complicated geometry of the domain, which requires special attention to the boundary conditions. We have employed the following discretization:

$$\left[\nabla^2 \mathbf{v}\right]_{i,j,k} = \frac{1}{\Delta x^2} \sum_{(i',j',k') \in I} \chi_{i+i',j+j',k+k'} \left(\mathbf{v}_{i+i',j+j',k+k'} - \mathbf{v}_{i,j,k}\right)$$

where $\chi_{i,j,k} = 1$ if the grid point (i,j,k) is within the domain and 0 otherwise, and the neighbourhood template is $I = \{(-1,0,0),(1,0,0),(0,-1,0),(0,1,0),(0,0,-1),(0,0,1)\}$. The space grid is regular with step Δx, rectangular $N_x \times N_y$ in the horizontal direction, and with $k \in \{1,\ldots,N_z(i,j)\}$ where $N_z(i,j)$ represents the thickness profile. In all our examples, $N_z(i,j)$ takes only two values, denoted as $N_{z,1}$ and $N_{z,2}$. The discretization parameters used for different results are described in Table II.

Figure	Δt	Δx	N_x	N_y	$N_{z,1}/N_{z,2}$
1	6.4×10^{-4}	8×10^{-2}	400	400	$20/40$
2(c)	6.4×10^{-4}	8×10^{-2}	400	400	$1/2, 2/3, 2/4, 3/4, 3/5, 4/5, 4/6, 6/7, 9/10, 14/15, 18/20, 19/20, 38/40, 40/80, 76/80$
2(f)	1.5×10^{-3}	0.25	200	200	$1/2, 2/4, 3/5, 4/6, 9/10, 18/20, 38/40, 76/80, 2/3, 3/4, 4/5, 6/7, 14/15, 19/20, 40/80$
3(d)	6.4×10^{-4}	8×10^{-2}	400	800	$5/6$
4(b)	1.5×10^{-3}	0.25	200	200	$5/6$

TABLE II. Discretization parameters in 3D simulations

Response function computations

For `DXSpiral` computations of the FitzHugh-Nagumo model, we use disk radius $\rho_{\max} = 25$, number of radial intervals $N_\rho = 1280$ and number of azimuthal intervals $N_\theta = 64$. For the Oregonator model, we have correspondingly $\rho_{\max} = 15$, $N_\rho = 128$ and $N_\theta = 64$. Density plots of the spiral wave solutions and the corresponding response functions are illustrated in Fig. 5.

Initial conditions

We initiated a spiral wave in a large square domain using the phase distribution method, as described e.g. in V.N. Biktashev, A.V. Holden "Re-entrant waves and their elimination in a model of mammalian ventricular tissue" *Chaos*, **8**(1):48–56 (1998), with the centre of the Archimedian spiral phase distribution at the centre of the square. A spiral wave initiated in that way was allowed to fully establish itself during a few rotations without any perturbations, and then saved to a disk file, to be used as an initial condition in 2D simulations, cutting its 2D domain to size as appropriate. The scroll waves for 3D simulations were

obtained from the same spiral wave, by extending it in the z direction. Hence in all cases we started with a spiral/scroll wave near the centre of the domain, and variation of the relative position of the initial spiral/scroll and a geometry feature was done by variation of the feature. Placing the scroll wave, formed effectively in an infinite medium, into new geometic constraints did of course cause some initial fast transient while establishing its transmural structure before proceeding with the slow drift in the long dimensions. This transient appeared as a slight deviation of the tip trajectory compared to what it would be expected otherwise, during one or two initial rotation periods. This small deviation is not noticeable on the figures at the resolution we use in this paper, so we did not find it useful to eliminate or isolate this transient from the output data.